High Bandwidth Voltage and Current Control Design for Voltage Source Converters

Arindam Ghosh and Gerard Ledwich
School of Engineering Systems
Queensland University of Technology
Brisbane, Australia
a.ghosh@qut.edu.au

***Abstract*: In this paper, two different high bandwidth converter control strategies are discussed. One of the strategies is for voltage control and the other is for current control. The converter, in each of the cases, is equipped with an output passive filter. For the voltage controller, the converter is equipped with an LC filter, while an output has an LCL filter for current controller. The important aspect that has been discussed the paper is to avoid computation of unnecessary references using high-pass filters in the feedback loop. The stability of the overall system, including the high-pass filters, has been analyzed. The choice of filter parameters is crucial for achieving desirable system performance. In this paper, the bandwidth of achievable performance is presented through frequency (Bode) plot of the system gains. It has been illustrated that the proposed controllers are capable of tracking fundamental frequency components along with low-order harmonic components. Extensive simulation results are presented to validate the control concepts presented in the paper.**

***Index Terms*: Voltage Source Converters, Voltage Control, Current Control, Bandwidth, Bode Plot.**

I. Introduction

POWER ELECTRONIC dc-ac converters are either current source type or voltage source type. Current source inverters (or converters) convert dc current to ac voltages, while voltage source converters (VSCs) convert dc voltages into ac voltages. Many of the distributed generators (DGs), like solar photovoltaic (PV) cells, fuel cells, produce dc voltages. Others, like wind, tidal, produce ac voltages with varied frequency and cannot be directly connected to the grid. Their output voltages are therefore rectified to produce dc voltages, which are converted ac voltages by the converter. Therefore voltage source converters are commonly used for grid connection of DGs [1-3].

In this paper, we shall investigate the structure and control of voltage source converters (VSCs). A VSC, being a switching device, can introduce harmonics in the system due switching of power semiconductors. To suppress these harmonics, passive filter circuits are used. Therefore the VSC controller should be designed such that the overall filter-converter circuit is dynamically stable. In this paper, state feedback based switching controller design both for voltage and current tracking are discussed. The closed-loop bandwidth of the converter-filter structure is analyzed using Bode plot. It will be highlighted how the desired tracking performance can be obtained by tuning the high pass filter gains. Extensive simulation results are presented to validate the proposals.

II. Converter and Filter Structure

A single-phase full bridge VSC that is supplying an RL load is shown in Fig. 1. The converter dc side is supplied by a voltage source V_{dc}. The converter contains four switches S_1 to S_4. The switches in each leg are complementary, i.e., when S_1 is S_4 is off and vice versa. The main idea is to control the switches such are a desired current is tracked through i or a desired voltage is produced across the terminals AB. The aim of the converter control is to generate the switching signal $u = \pm 1$.

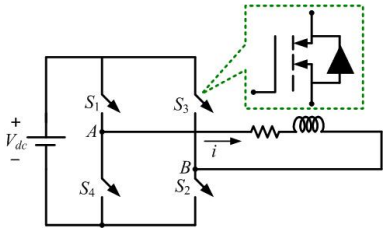

Fig. 1. A single-phase voltage source converter structure.

The single-phase equivalent circuit of a converter, with its associated filter, is shown in Fig. 2. Two types of filters are commonly used – inductance-capacitance (LC) type and inductance-capacitance-inductance (LCL) type. In Fig. 2, the filter inductors are denoted by L_1 and L_2, while the capacitor is denoted by C. The voltage across the capacitor is denoted by v_c. The resistances R_1 and R_2 are the associated with the inductances L_1 and L_2 respectively, arising due to their finite quality factor.

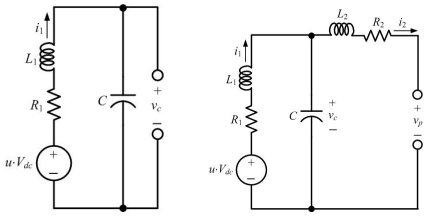

Fig. 2. Single-phase VSC equivalent circuit with (a) LC and (b) LCL filter.

III. Voltage Control with LC Filter

In this section, we shall discuss a voltage control strategy, for which the LC filter structure will be employed. We shall also present an example, which will highlight the design process.

A. State Feedback Control

Defining a state vector as $x^T = [v_c \quad i_1]$, the state space equation of the system can be written from Fig. 2 (a) as

$$\dot{x} = Ax + Bu_c \tag{1}$$

where u_c is the feedback control law, based on which the converter switching signal $u = \pm 1$ is generated and the matrices A and B are

$$A = \begin{bmatrix} 0 & 1/C \\ -1/L_1 & -R_1/L_1 \end{bmatrix}, \quad B = \begin{bmatrix} 0 \\ V_{dc}/L_1 \end{bmatrix}$$

There are various converter control strategies. However we shall adopt the linear quadratic regulator (LQR) based state feedback control. This was used in [4], where it was shown that hysteretic current control for such system can lead to an unstable operation. Assuming that the references for the states are available and are denoted by $x_{ref} = [v_{cref} \quad i_{1ref}]$, the state feedback control law is given as

$$u_c = -K\left(x - x_{ref}\right) \tag{2}$$

where $K = [k_1 \quad k_2]$ is the feedback gain matrix, which is computed based on LQR and design parameters. The schematic diagram of the control law is given in Fig. 3 (a).

The LC filter structure is most suitable for tracking the output voltage, where the voltage reference (v_{cref}) can be prespecified. However, it is rather difficult to find a reference (i_{1ref}) for the converter output current i_1. One approach can be to set this reference to zero. This will however lead to incorrect control action. To avoid this problem, a state transformation has been used in [4]. This is however feasible only when the overall system structure and rough estimates of the system parameters are known a priori. Therefore this solution cannot be stated as a general solution.

It should be noted that the current i_1 should only contain lower frequency components, while its high frequency components should be zero. Therefore, if we pass this current through a high-pass filter (HPH), then we expect the output (i_{1HPF}) of the filter to be zero. The HPF structure is given by

$$\frac{i_{1HPF}}{i_1} = \frac{s}{s+\alpha} \tag{3}$$

where α determines the cutoff frequency of the filter. The controller structure is with the HPF is shown in Fig. 3 (b).

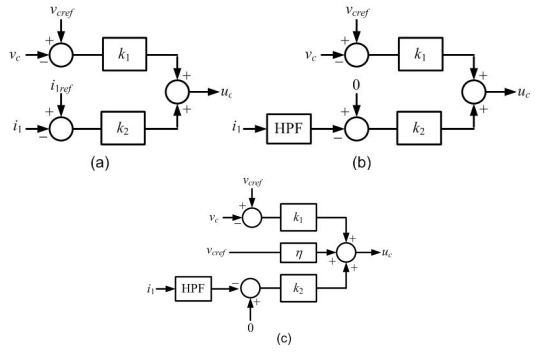

Fig. 3. Three different feedback control structures: (a) full state feedback, (b) partial state feedback with high-pass filter and (c) partial state feedback with feed forward control.

It may also be desirable to use a feed forward of the voltage reference in order to obtain better tracking characteristics. This is shown in Fig. 3 (c), where the reference voltage is multiplies by a constant η and is added to the feedback signals. In any of the control schemes, the converter switching pulses are obtained from the computed values of u_c. This is discussed next.

B. Pulse Width Modulated (PWM) Control

For the control of the VSC, we shall use a bi-polar switching strategy [5]. This is shown in Fig. 4. This consists of a triangular carrier waveform (v_{tri}), which varies from – 1 to + 1 with a duty ratio of 0.5 (Fig. 4 a). The control output is sampled twice in each cycle, one at the negative peak of the carrier waveform and once at the positive peak. The sampler is assumed to be an impulse modulator that consists of a train of pulses as shown in Fig. 4 (a). The control signal (u_c) is shown in Fig. 4 (c). The control signal is sampled by the sampler of Fig. 4 (b) and is held by a zero order hold (ZOH) circuit. The output u_c^* of the ZOH is shown in Fig. 4 (d), while its inverse ($-u_c^*$) is shown in Fig. 4 (e).

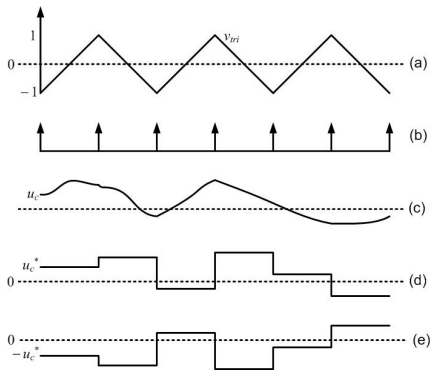

Fig. 4. PWM switching control: (a) carrier waveform, (b) sampler pulse train, (c) the control signal (d) sampled and ZOH output and (d) negative of the sampled and ZOH output.

The switching pulses ($u = \pm 1$) is generated by comparing u_c^* and $-u_c^*$ with the carrier waveform (v_{tri}). With respect to Fig. 1 for a single-phase inverter, the algorithm is given by

$$\begin{aligned} &\text{If } u_c^* > v_{tri} \text{ then } S_1 \text{ is ON} \\ &\text{elseif } u_c^* < v_{tri} \text{ then } S_1 \text{ is OFF} \\ &\text{If } u_c^* < v_{tri} \text{ then } S_4 \text{ is ON} \\ &\text{elseif } u_c^* > v_{tri} \text{ then } S_4 \text{ is OFF} \end{aligned} \tag{4}$$

$$\begin{aligned} &\text{If } -u_c^* > v_{tri} \text{ then } S_3 \text{ is ON} \\ &\text{elseif } -u_c^* < v_{tri} \text{ then } S_3 \text{ is OFF} \\ &\text{If } -u_c^* < v_{tri} \text{ then } S_2 \text{ is ON} \\ &\text{elseif } -u_c^* > v_{tri} \text{ then } S_2 \text{ is OFF} \end{aligned} \tag{5}$$

It can be seen from (4-5) that operations of the switch pairs S_1-S_4 and S_3-S_2 are complementary. However, in order to prevent both the switches of a leg to be ON at a given time (shoot through fault), a small delay, called the blanking period, is introduced between the operations of two switches of the same leg. Most commercial inverters automatically introduce the blanking period. However this period is not considered in this analysis.

C. Closed-Loop Converter Model

Ignoring delay, we can assume that the average over the switch period is obtained by a linear modulator as in [5]. The PWM amplifier can then be considered as an ideal unit gain amplifier, i.e., we can assume $u_c = u$. Under this condition, the open-loop is the same as given by (1). We now derive the closed-loop system model. Let us first consider the transfer function of the HPF, given by (3). This can be written as

$$i_{1HPF} = \left(\frac{s}{s+\alpha}\right) i_1 = \left(1 - \frac{\alpha}{s+\alpha}\right) i_1 = i_1 - i_{1LPF} \tag{6}$$

where i_{1LPF} is given by

$$i_{1LPF} = \left(\frac{\alpha}{s+\alpha}\right) i_1 \tag{7}$$

Equation (7) can be expressed in differential equation form as

$$\frac{d}{dt} i_{1LPF} = -\alpha i_{1LPF} + \alpha i_1 \tag{8}$$

Let us now define a new state vector as $x_e{}^T = [v_c \quad i_1 \quad i_{1LPF}]$. Then combining (1) with (8), we get an augmented state space equation of the form

$$\dot{x}_e = A_e x_e + B_e u_c \tag{9}$$

where

$$A_e = \begin{bmatrix} A & 0 \\ [0 \quad \alpha] & -\alpha \end{bmatrix} \text{ and } B_e = \begin{bmatrix} B \\ 0 \end{bmatrix}$$

The discrete-time equivalent (9) is given as

$$x_e(k+1) = F x_e(k) + G u_c(k) \tag{10}$$

where k is the time index and the matrices F and G are [6]

$$F = e^{A_e \Delta T}, \quad G = \int_0^{\Delta T} e^{A_e t} B_e dt, \quad \Delta T = \text{Sampling interval}$$

From Fig. 3 (c), the feedback control law is given by

$$u_c(k) = (\eta + k_1) v_{cref}(k) - k_1 v_c(k) - k_2 i_{1HPF}(k) \tag{11}$$

Substituting (6) in (11), we get

$$\begin{aligned} u_c(k) &= (\eta + k_1) v_{cref}(k) - k_1 v_c(k) - k_2 i_1(k) + k_2 i_{1LPF}(k) \\ &= -[k_1 \quad k_2 \quad -k_2] x_e(k) + (\eta + k_1) v_{cref}(k) \end{aligned} \tag{12}$$

Combining (12) with (10), the closed-loop state equation is given by

$$x_e(k+1) = (A_e - B_e [k_1 \quad k_2 \quad -k_2]) x_e(k) + (\eta + k_1) B_e v_{cref}(k) \tag{13}$$

D. Numerical Examples

Let us consider the system shown in Fig. 5 in which the converter is connected with an RL plus back emf load. The system parameters used and their definition are given in Table 1. The frequency of the triangular waveform (v_{tri}) is taken as 15 kHz and the sampling frequency is chosen twice of this frequency, i.e., 30 kHz. The frequency response of the open-loop system, which contains only the LC filter dynamics of (1), is shown in Fig. 6. It is obvious that the filter resonates around 2.2 kHz.

TABLE 1: SYSTEM PARAMETERS WITH LC FILTER

System Quantities	Parameter values
System frequency	50 Hz
Back emf (v_s)	230 V (rms)
Load resistance (R_s)	5 Ω
Load inductance (L_s)	11.6 mH
Filter capacitance (C)	25 μF
Filter inductance (L_1)	0.2 mH
Filter resistance (R_1)	0.1 Ω
DC voltage (V_{dc})	350 V

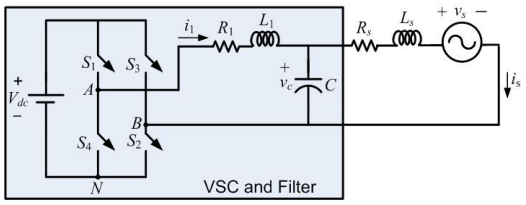

Fig. 5. H-bridge VSC with LC filter connected to an RL plus back emf load.

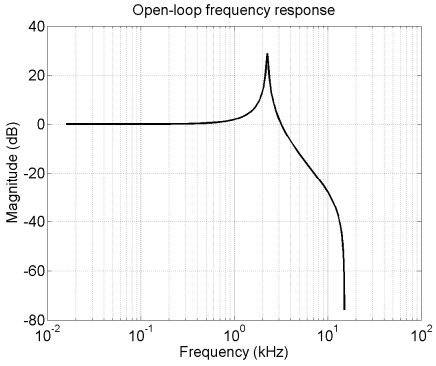

Fig. 6. Open-loop frequency response with LC filter.

The closed-loop frequency response, for various values of HPF coefficient α, is shown in Fig. 7. In this, the input is the voltage reference v_{cref} and the output is the capacitor voltage v_c. It can be seen that for a = 500, the circuit behaves like an ideal amplifier with a gain of 0 dB (i.e., $v_{cref} = v_c$) till around 3 kHz. The 3 dB cut-off frequency is around 6.5 kHz, indicating that the converter-filter system will track a voltage reference up to this frequency. The tracking error however increases as α increase. However, it is still less than 2 dB, indicating a maximum tracking error of 20%.

The phase of the closed-loop system, for two values of α, is shown in Fig. 8. It can be seen that the phase shift between the reference and output voltages is almost zero when the system frequency is 100 Hz or less. This implies that the converter is able to track a reference waveform of 50 Hz without any appreciable phase shift. However, the phase shift increases as the system frequency increases. Also note that the phase shift is more for lower values of α. From Figs. 7 and 8, it is evident that α = 500 is sufficient for tracking fundamental frequency (50 Hz) waveforms. However, for higher frequency tracking, this value has to chosen as a compromise between phase error and magnitude error.

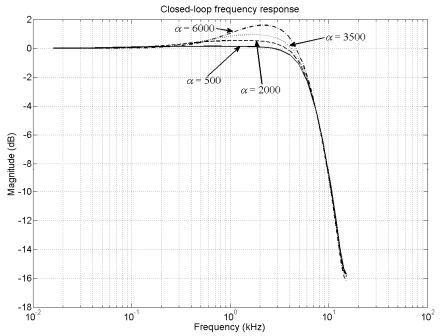

Fig. 7. Closed-loop frequency response for various values of α.

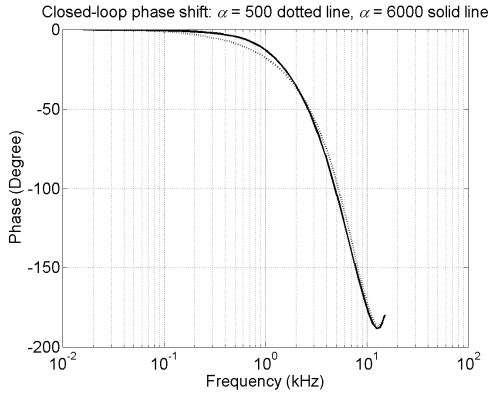

Fig. 8. Closed-loop phase shift for two values of α.

The H-bridge converter switching behavior is shown in Fig. 9. The intersection of the sampled control signal u_c^* and its negative with the 15 kHz triangular waveform is shown in the top sub-plot. As evident from Fig. 5 and (4), the voltage (v_{AN}) across the first leg is generated from the intersection of u_c^* and v_{tri}. Similarly the voltage (v_{BN}) across the second leg is generated from the intersection of $-u_c^*$ and v_{tri}. The difference between v_{AN} and v_{BN} gives the converter output voltage, which can take on values of $+V_{dc}$ (350 V), $-V_{dc}$ (– 350 V) and 0 V. The converter leg and output voltages are also shown in Fig. 9.

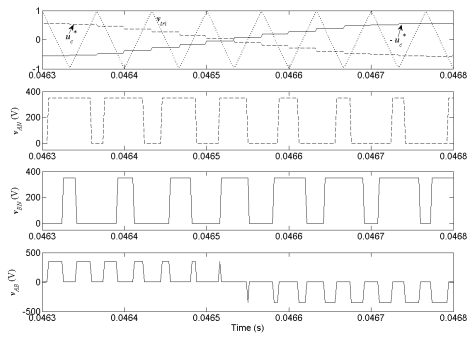

Fig. 9. H-bridge converter switching behavior.

To evaluate the performance of voltage tracking, we consider the system of Fig. 5, the data for which are given in Table 1. First we assume that the converter is required to track a 50 Hz voltage waveform with a peak of 230 V. The HPF coefficient is chosen as α = 500. The system performance is shown in Fig. 10. The reference and converter output voltages are shown in Fig. 10 (a). The error between these two voltages is shown in Fig. 10 (b). It can be seen that the peak of the tracking error is around 10 V.

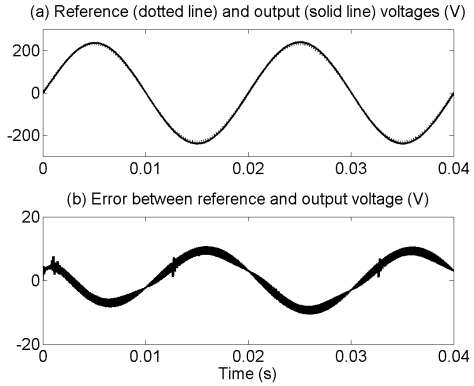

Fig. 10. Voltage tracking performance for a 50 Hz reference voltage.

Let us now choose a reference voltage that contains odd harmonics up to the order 19 and an additional 31st harmonics. The reference wave is given by

$$v_{cref} = 150 \times \left[\sum_{k=1,3,\ldots 19} \frac{\sin(k\omega t)}{k} + 0.2\sin(31\omega t) \right]$$

The reference voltage waveform is shown in Fig. 11 (a). The voltage tracking error for an α of 500 is shown in Fig. 11 (b), while that for an α of 6000 is shown in Fig. 11 (c). It can be seen that the magnitude of the tracking error is considerably less when high filter coefficient is chosen, which reduces the phase error – the major contributor of the tracking error.

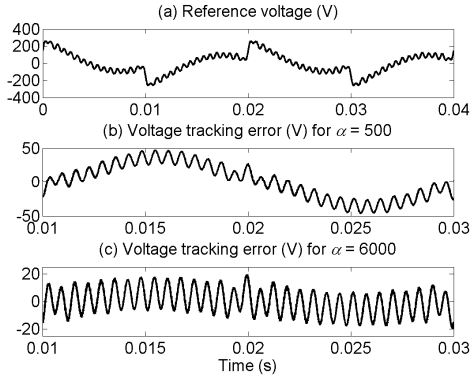

Fig. 11. Voltage tracking performance for a distorted reference voltage.

IV. Current Control with LCL Filter

In this section, we shall highlight the control of converters with LCL filters. In particular, this structure is useful for current control, where the current to be injected is pre-specified.

A. Closed-loop Converter Model

The single-phase equivalent circuit of the converter with LCL filter is shown in Fig. 2 (b). With respect to this figure, we define a state vector as $x^T = [v_c \quad i_1 \quad i_2]$. The state space equation of the system can be written as

$$\dot{x} = Ax + Bu_c + Dv_p \tag{14}$$

$$A = \begin{bmatrix} 0 & 1/C & -1/C \\ -1/L_1 & -R_1/L_1 & 0 \\ 1/L_2 & 0 & -R_2/L_2 \end{bmatrix}, B = \begin{bmatrix} 0 \\ V_{dc}/L_1 \\ 0 \end{bmatrix}, D = \begin{bmatrix} 0 \\ 0 \\ -1/L_2 \end{bmatrix}$$

The purpose of the control is to track a reference current i_{2ref}. We shall therefore use two HPFs, one for i_1 and the other for v_c. The HPFs are derived in the same fashion as (6-8). They are

HPF-1 for i_1:

$$i_{1HPF} = \left(\frac{s}{s+\alpha_1}\right) i_1 = \left(1 - \frac{\alpha_1}{s+\alpha_1}\right) i_1 = i_1 - i_{1LPF} \tag{15}$$

where i_{1LPF} is given by

$$i_{1LPF} = \left(\frac{\alpha_1}{s+\alpha_1}\right) i_1 \tag{16}$$

Equation (15) can be expressed in differential equation form as

$$\frac{d}{dt} i_{1LPF} = -\alpha_1 i_{1LPF} + \alpha_1 i_1 \tag{17}$$

HPF-2 for v_c:

$$v_{cHPF} = \left(\frac{s}{s+\alpha_2}\right) v_c = \left(1 - \frac{\alpha_2}{s+\alpha_2}\right) v_c = v_c - v_{cLPF} \tag{18}$$

where v_{cLPF} is given by

$$v_{cLPF} = \left(\frac{\alpha_2}{s+\alpha_2}\right) v_c \tag{19}$$

Equation (18) can be expressed in differential equation form as

$$\frac{d}{dt} v_{cLPF} = -\alpha_2 v_{cLPF} + \alpha_2 v_c \tag{20}$$

Let us now define a new state vector as $x_e{}^T = [v_c \;\; i_1 \;\; i_2 \;\; v_{cLPF} \;\; i_{1LPF}]$. Then combining (14), (17) and (20), we get an augmented state space equation of the form

$$\dot{x}_e = A_e x_e + B_e u_c + D_e v_p \tag{21}$$

where

$$A_e = \begin{bmatrix} A & & 0 \\ \begin{bmatrix} \alpha_2 & 0 & 0 \\ 0 & \alpha_1 & 0 \end{bmatrix} & & \begin{bmatrix} -\alpha_2 & 0 \\ 0 & -\alpha_1 \end{bmatrix} \end{bmatrix}, \; B_e = \begin{bmatrix} B \\ 0 \\ 0 \end{bmatrix}, \; D_e = \begin{bmatrix} C \\ 0 \\ 0 \end{bmatrix}$$

The closed-loop control scheme is shown in Fig. 12. From this figure, the control law is given as

$$\begin{aligned} u_c &= -k_1 v_{cHPF} - k_2 i_{1HPF} + k_3 (i_{2ref} - i_2) \\ &= -k_1 v_c + k_1 v_{cLPF} - k_2 i_1 + k_2 i_{1LPF} + k_3 (i_{2ref} - i_2) \\ &= -[k_1 \;\; k_2 \;\; k_3 \;\; -k_1 \;\; -k_2] x_e + k_3 i_{2ref} \end{aligned} \tag{22}$$

Combining (19) and (20), the closed-loop state equation is given by

$$\dot{x}_e = (A_e - B_e [k_1 \;\; k_2 \;\; k_3 \;\; -k_1 \;\; -k_2]) x_e + k_3 B_e i_{2ref} + D_e v_p \tag{23}$$

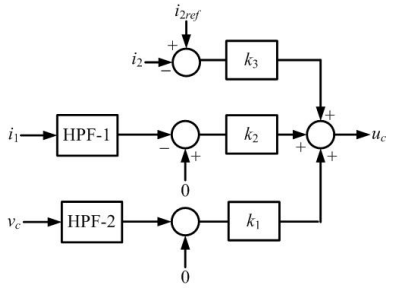

Fig. 12. The current control structure.

B. Numerical Examples

Let us consider the same system as given in Fig. 13. The system data are given in Table 2. Let us first assume that we have the full system knowledge (i.e., the knowledge of the load resistance and inductance). In this event, v_p becomes equal to v_s and the matrix A of (14) is altered to include the load resistance and inductance as

$$A = \begin{bmatrix} 0 & 1/C & -1/C \\ -1/L_1 & -R_1/L_1 & 0 \\ 1/(L_2 + L_s) & 0 & -(R_1 + R_2)/(L_2 + L_s) \end{bmatrix}$$

The controller gains, obtained with the full system knowledge, are

$$K = [12.6254 \quad 19.6589 \quad 2661]$$

TABLE II: SYSTEM PARAMETERS WITH LCL FILTER

System Quantities	Parameter values
System frequency	50 Hz
Back emf (v_s)	230 V (rms)
Load resistance (R_s)	5 Ω
Load inductance (L_s)	11.6 mH
Filter capacitance (C)	25 μF
Inside filter inductance (L_1)	0.2 mH
Inside filter resistance (R_1)	0.1 Ω
Outside filter inductance (L_2)	1.25 mH
Outside filter resistance (R_2)	0.1 Ω
DC voltage (V_{dc})	450 V
HPF-1 (α_1)	5000
HPF-2 (α_2)	5000

The closed-loop frequency response, as per the discrete-time equivalent of (23), is shown in Fig. 14. It can be seen that the magnitude has a unit gain below 300 Hz and it starts rolling off above 5 kHz. The system response while tracking a fundamental frequency waveform with a peak of 25 A is

shown in Fig. 15 (a), while the tracking error is shown in Fig. 15 (b). It can be seen that tracking error, barring some distortion at the peaks of the waveform, is negligible. The distortions at the peaks can be minimized by increasing the dc bus voltage. This may however be not always possible.

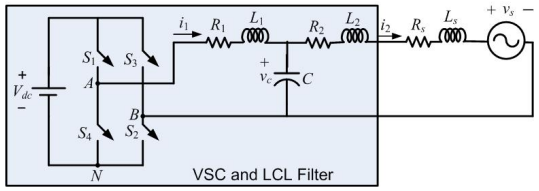

Fig. 13. H-bridge converter with LCL filter connected to an RL plus back emf load.

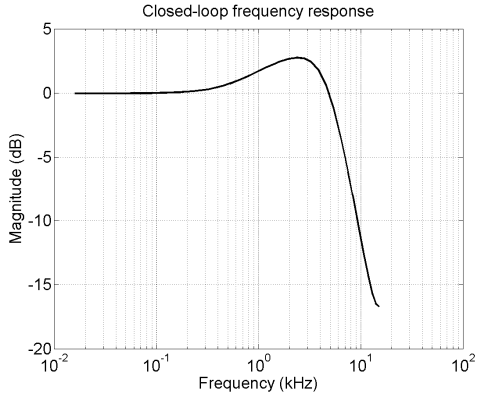

Fig. 14. Closed-loop frequency response with LCL filter.

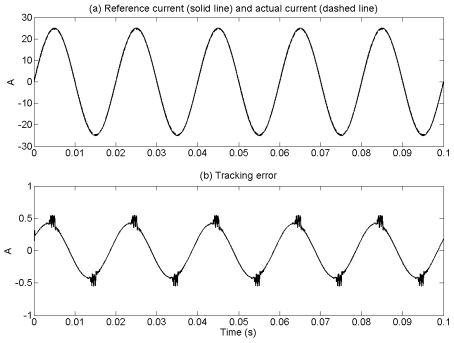

Fig. 15. Current tracking with full system knowledge.

The problem with the design mentioned above is that it is not possible to estimate the load or the back emf most of the time. We therefore have to design the controller based on the available filter data (i.e., through 23). From the LQR design, these gains are given as

$$K = \begin{bmatrix} 17.16 & 19.27 & 428.88 \end{bmatrix}$$

We now know that the current will be injected in series with an equivalent circuit with a large enough inductor. Therefore in order to have a better current tracking, the output inductor gain is increased and the gains associated with the inner inductor and the filter capacitor are decreased. The controller gains are then modified to

$$K = \begin{bmatrix} 5 & 10 & 1000 \end{bmatrix}$$

The system tracking performance with the modified controller gains is shown in Fig. 16. Comparing with Fig. 15, it can be seen that the tracking error has increased. However, since the peak error is below 1 A, the tracking performance is acceptable. In general, a current tracking can work perfectly if the current flows through a low impedance path. However, when the current has to flow through a relatively large inductor, the controller has to work harder and may saturate. This problem does occur with a voltage controller, which directly controls the voltage across the shunt connected capacitor.

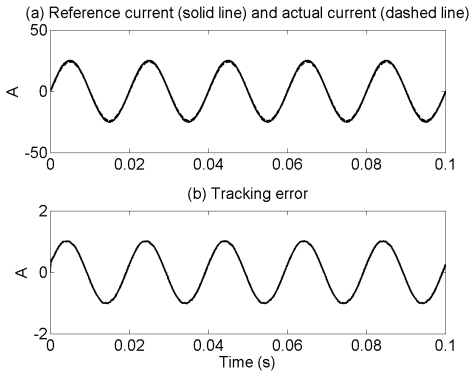

Fig. 16. Current tracking with incomplete system knowledge.

V. Conclusions

The paper presents techniques for converter control. Two different converter-filter structures are considered. Two separate controller design principles are presented, one for each filter structure. The bandwidth issues of the filters are also discussed. From the presented results and discussion, it can be surmised that voltage controller has a better tracking performance than a current tracker. In this paper, we have only presented the single-phase performance of the converters, since most of the distributed energy resources (e.g., PV, hybrid electric vehicles etc) will be connected to the grid through such converters. However the analysis and design principles presented are general in nature and can be extended to include three-phase converters.

Acknowledgement

The authors acknowledge CSIRO Cluster on Intelligent Grid for the financial support to conduct this research.

References

[1] R. Majumder, A. Ghosh, G. Ledwich and F. Zare, "Load sharing and power quality enhanced operation of a distributed microgrid," IET Renewable Power Generation, Vol. 2, No. 3, pp. 109-119, June, 2009.

[2] M. N. Marwali, M. Dai; A. Keyhani, "Robust stability analysis of voltage and current control for distributed generation systems" IEEE Trans. on Energy Conversion, Vol. 21, Issue-2, pp. 516-526, 2006.

[3] M. Reza, D. Sudarmadi, F. A. Viawan, W. L. Kling, and L. Van Der Sluis, "Dynamic Stability of Power Systems with Power Electronic Interfaced DG," Power Systems Conference and Exposition, PSCE'06, pp. 1423-1428, 2006.

[4] A. Ghosh and G. Ledwich, "Load compensating DSTATCOM is weak ac systems," IEEE Trans. Power Delivery, Vol. 18, No. 4, pp. 1302-1309, 2003.

[5] N. Mohan, T. M. Undeland and W. P. Robbins, 3rd Ed., *Power Electronics: Converters*, *Applications and Design*, John Wiley, New York, 2003.

[6] B. C. Kuo, *Digital Control Systems*, Holt-Saunders, Tokyo, 1980.